Theory and Implementation of RF-Input Outphasing Power Amplification

Citation: Barton, Taylor W., and Perreault, David J. "Theory and Implementation of RF-Input Outphasing Power Amplification." IEEE Transactions on Microwave Theory and Techniques 63, 12 (December 2015): 4273–4283 © 2015 Institute of Electrical and Electronics Engineers (IEEE)

As Published: http://dx.doi.org/10.1109/tmtt.2015.2495358

Publisher: Institute of Electrical and Electronics Engineers (IEEE)

Persistent URL: http://hdl.handle.net/1721.1/111633

Version: Author's final manuscript: final author's manuscript post peer review, without publisher's formatting or copy editing

IEEE Transactions on Microwave Theory and Techniques, Vol. 63, No. 12, pp. 4273-4283, December 2015.

Theory and Implementation of RF-Input Outphasing Power Amplification

Taylor W. Barton, *Member, IEEE,* and David J. Perreault, *Fellow, IEEE*

***Abstract*—Conventional outphasing power amplifier systems require both an RF carrier input and a separate baseband input to synthesize a modulated RF output. This work presents an RF-input / RF-output outphasing power amplifier that directly amplifies a modulated RF input, eliminating the need for multiple costly IQ modulators and baseband signal component separation as in previous outphasing systems. An RF signal decomposition network directly synthesizes the phase- and amplitude-modulated signals used to drive the branch PAs. With this approach, a modulated RF signal including zero-crossings can be applied to the single RF input port of the outphasing RF amplifier system. The proposed technique is demonstrated at 2.14 GHz in a four-way lossless outphasing amplifier with transmission-line power combiner. The RF decomposition network is implemented using a transmission-line resistance compression network with nonlinear loads designed to provide the necessary amplitude and phase decomposition. The resulting proof-of-concept outphasing power amplifier has a peak CW output power of 93 W, peak drain efficiency of 70%, and performance on par with a previously-demonstrated outphasing and power combining system requiring four *IQ* modulators and a digital signal component separator.**

***Index Terms*—base stations, outphasing, power amplifier (PA), Chireix, LINC, load modulation, signal component separator, transmission-line resistance compression network.**

I. Introduction

Outphasing architectures use phase-shift control of multiple saturated or switched-mode branch power amplifiers (PAs) to create a modulated RF output. Interaction through a lossless non-isolating power combiner produces load modulation of the branch amplifiers, which in turn modulates the system output power. When realized with efficient saturated or switched-mode branch amplifiers, the outphasing approach has the potential to provide high operating efficiency over a wide range of output power levels, making it ideal for high peak-to-average power ratio (PAPR) signals such as those found in modern communications systems. Examples of this approach include Chireix power combining systems [1]–[5], and the multi-way lossless outphasing system [6]–[11] which improves upon the achievable operating efficiency of the Chireix system by providing nearly ideal resistive loading conditions to the branch PAs.

Manuscript received June 30, 2015; revised October 24, 2015.

This paper is an expanded version from the IEEE MTT-S International Microwave Symposium, Phoenix, AZ, USA, 17-22 May 2015.

T. Barton is with the Department of Electrical Engineering, The University of Texas at Dallas, Richardson, TX 75080. (email: taylor.barton@utdallas.edu)

D. Perreault is with the Department of Electrical Engineering and Computer Science, Massachusetts Institute of Technology, Cambridge, MA 02139. (email: djperrea@mit.edu)

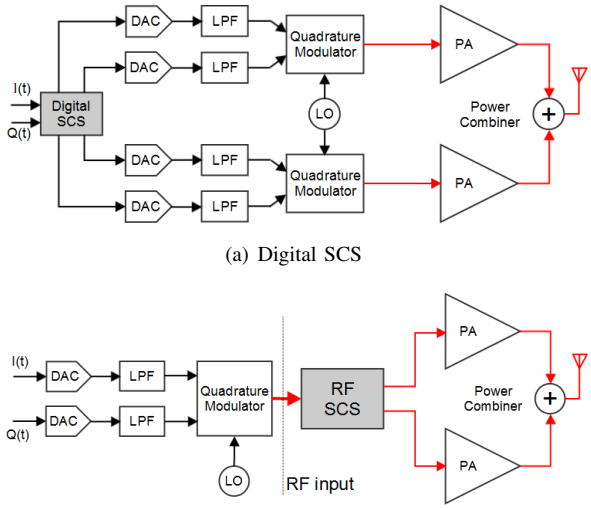

(a) Digital SCS

(b) RF-domain SCS (this work)

Fig. 1. Comparison of signal component separation techniques for conventional outphasing systems and the RF-domain SCS proposed in this work. Baseband signals are indicated with black lines while RF paths are shown in red. The RF-input outphasing PA has reduced cost, complexity, and power consumption and can operate directly on a modulated RF input.

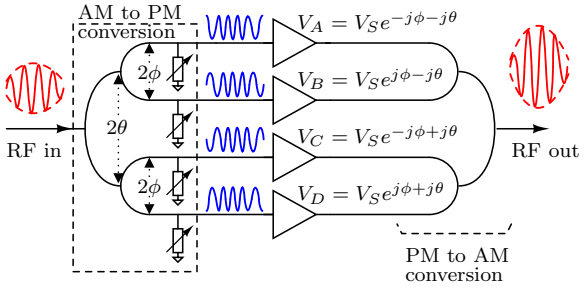

Fig. 2. Conceptual schematic of the four-way RF-input outphasing system, with example waveforms sketched assuming the PA is operating in the outphasing regime. The phasor relationship among the four branch voltages V_A–V_D is a result of the decomposition network structure. The non-isolating combining and decomposition networks are abstracted for simplicity.

Since its introduction by Chireix in 1935, a major limitation in the outphasing approach has been the need for signal component separation of the desired RF signal into multiple phase- and amplitude-modulated signals driving the branch PAs. For example, in an early commercial outphasing amplifier, Ampliphase, two sets of dynamic phase-modulating amplifiers were used to modulate the carrier signal by the (baseband) audio signal and drive the branch PAs [12]. This

property has made outphasing systems less attractive compared to the Doherty approach with its ability to operate directly on a modulated RF input signal [13], [14].

The signal component separator (SCS) and the associated need for multiple baseband-to-RF upconverting paths incurs excessive complexity, cost, and power consumption to the outphasing system compared to power amplifiers that can operate directly on a modulated RF input. The digital signal decomposition requirement can also complicate any digital correction scheme. SCS approaches performing the required computation have been proposed in various domains, including analog baseband [15] and analog IF operating in feedback [16]–[18] or open-loop [19] topologies. The most common approach in modern outphasing systems, however, is to use some form of digital signal processing based on lookup tables or other means of computing the nonlinear relationship between the input signal and the phase-modulated branch PA drives [20]–[25]. As illustrated in the block-diagram comparison in Fig. 1, performing the SCS in the RF domain instead of the digital domain allows for decoupled design of the digital and RF elements, reduced system complexity, and for the resulting outphasing system to be treated as a "black box" drop-in replacement for another PA.

This work presents an RF-input / RF-output outphasing PA, shown in block diagram form in Fig. 2. An RF-domain signal decomposition network directly synthesizes the multiple branch PA drive signals from a modulated RF input signal, performing both the phase and amplitude modulation required for outphasing systems to control the output power over a wide range [3], [9]. This signal decomposition network (or RF-domain signal component separator) is based on use of a resistance compression network (RCN) terminated with nonlinear elements. The resulting system is a true RF amplifier in the sense that its input is a modulated RF signal, and its output is an amplified version of that signal.

This paper expands on the brief conference paper [26] with a complete analysis of the theory and development of this approach, and presents additional experimental data including modulated output spectrum and input impedance characterization of the 2.14-GHz prototype system. In Section II we derive the theoretical behavior of the RF decomposition network, and describe how a nonlinear termination network is used to implement mixed-mode phase- and amplitude modulation of practical outphasing systems. Design of the nonlinear termination network and RF decomposition networks is discussed in Section III. Finally, the experimental system showing proof-of-concept operation at a 2.14 GHz carrier frequency with peak output power of 95 W is described in Section IV.

II. System Theory

Fig. 3 shows a simplified schematic of the proposed RF-input / RF-output system, in which a passive RF decomposition network performs signal separation of a modulated input to produce the four modulated signals required to drive the four branch PAs. The system consists of the decomposition network (based on a four-way transmission-line resistance compression network (TLRCN) terminated with nonlinear components), driver and branch PAs, and a lossless multi-way power combiner.

A. Conceptual Overview

In the outphasing operating mode, the function of the RF signal decomposition network is to convert amplitude modulation at the system input into relative phase modulation among the inputs to the four branch PAs. As can be seen from the structure in Fig. 3, the signal decomposition is related to the combining network through symmetry. Conceptually, the decomposition network's function can be thought of as being opposite of that of the combining network. That is, in the power combining network, phase-modulated signals interact to produce amplitude modulation at the output, whereas in the signal decomposition network, input amplitude modulation is converted to four phase-modulated drive signals. The four outphased drive signals are chosen such that the branch PAs "see" loading conditions that vary (nearly resistively) over some pre-determined range. Extending the conceptual symmetry argument, then, varying the decomposition network's loads over that same range of resistance values should (at least approximately) generate the desired outphasing relationship among the four port phases. The nonlinear loads (R_{NL} in Fig. 3) are designed to vary as a function of input amplitude so that amplitude modulation at the input is converted "automatically" to phase modulation among the four PA drive signals. This inverse RCN (IRCN) outphasing control strategy forms the basis of the RF signal decomposition in the outphasing regime.

The implementation described in this work and used for the experimental prototype is based on an all-transmission-line approach as described for the power combining system in [10], and for resistance compression networks (RCNs) in [27], but we note that versions are also possible using discrete components, microstrip techniques, or a combination of those, related to the lumped-element [7], [8], microstrip with shunt reactive element [9], and all-transmission-line [10] variations of the four-way outphasing power combiner. Likewise, the approaches described in this work may be applied two-way (Chireix) outphasing, including its relatively wideband variations [4], [5]. The four-way outphasing architecture is selected as the basis for this work due to both its nearly-resistive loading conditions presented to the branch PAs (which lends itself to an intuitive understanding of the RF-input approach by arguments of symmetry) and because the impact of eliminating the multiple upconvering paths including mixers and filters is even greater in the four-way system compared to the conventional Chireix approach.

B. Outphasing Operation

An IRCN outphasing control law was originally introduced as one basis for selecting the input phases θ and ϕ for a baseband-input, lumped-element four-way outphasing system [6]. This control law is based on the approximate relationship between the phase angles of a multi-way RCN and a corresponding multi-way power combining network with appropriate controls: the power combiner can be (approximately)

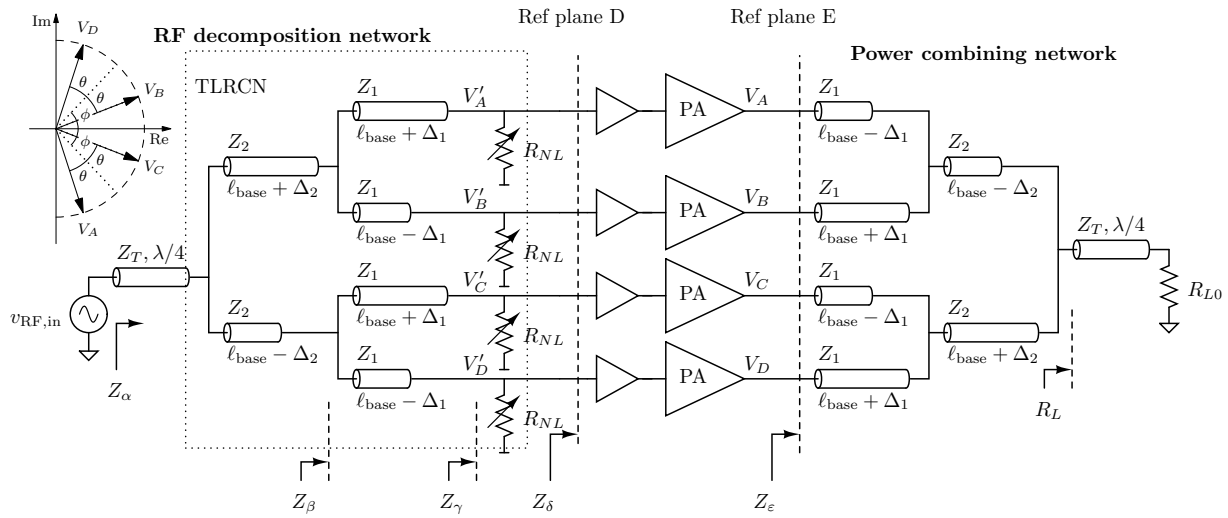

Fig. 3. Simplified schematic of the new RF-input / RF-output outphasing system showing the transmission-line based implementation used in the experimental prototype in this work. The vector diagram at upper left describes the relative phase relationship among the four branch signals V_A–V_D, given also by (1)–(4).

derived from an RCN by applying the principle of time-reversal duality [6]. In essence, the direction of power flow in the power combining network is reversed by changing the sign of each reactance, resistance, and electrical length, replacing sources (approximated as negative resistors) with resistors (and vice versa). This transformation is illustrated for the lumped-element combiner of [6] in Fig. 4. An analogous inverse-RCN approach can be seen in the relationship between the transmission-line combining network [10] and transmission-line resistance compression network (TLRCN) [27]. As described in detail in [27], a TLRCN may be constructed as a binary tree of transmission-line sections, with the two branch lengths at the nth branch point a deviation $\pm\Delta_n$ from a base length (typically $\lambda/2$ or $\lambda/4$). The ends of the final branches are typically terminated in identical loads, and a quarter-wave transmission line may also be employed before the initial branch point to provide impedance matching into the TLRCN.

Examining the RF decomposition network of Fig. 3, we can see that it is based on a passive network (derived from a TLRCN) terminated with four varying (but equal) resistances R_{NL}. In the following analysis, we assume that the TLRCN terminating impedance is $Z_\gamma = R_{NL}$, neglecting any effects of the input impedance Z_δ. In practice, as will be shown in Section III below, the terminating impedance can be designed to include effects of Z_δ. The four output port voltages V'_A – V'_D can be found in terms of the input $V_{\text{RF,in}}$, terminating resistances R_{NL}, and network parameters through analysis of the decomposition network (1)–(2). These relationships are derived in the Appendix. Note that in (2), Z_β represents the impedance into the transmission-line pairs closest to the nonlinear loads R_{NL} (see Fig. 3) and is a function of R_{NL}. From [27], Z_β will be purely resistive when R_{NL} is resistive.

$$\begin{bmatrix} V'_A \\ V'_B \\ V'_C \\ V'_D \end{bmatrix} = V_{in} \frac{R_{NL}}{\sqrt{Z_1^2 \sin^2\sigma_1 + R_{NL}^2 \cos^2\sigma_1}} \times \frac{Z_\beta}{\sqrt{Z_2^2 \sin^2\sigma_2 + Z_\beta^2 \cos^2\sigma_2}} \begin{bmatrix} e^{-j\phi}e^{-j\theta} \\ e^{+j\phi}e^{-j\theta} \\ e^{-j\phi}e^{+j\theta} \\ e^{+j\phi}e^{+j\theta} \end{bmatrix} \quad (1)$$

$$Z_\beta = \frac{1}{2(1+\tan^2\sigma_1)} \left(R_{NL} + \frac{Z_1^2}{R_{NL}} \tan^2\sigma_1 \right) \quad (2)$$

The phases of the four port voltages are related as indicated in (1) and the vector diagram in Fig. 3, and can be shown to be related to the load resistance R_{NL} as in (3)–(4) where $Z_2 = Z_1$, $\ell_{base} = \lambda/2$, $\sigma_1 = 2\pi\Delta_1/\lambda$, and $\sigma_2 = 2\pi\Delta_2/\lambda$, with Δ_1 and Δ_2 representing differences in base line lengths as illustrated in Fig. 3.

$$\theta = \tan^{-1}\left(2Z_1 \tan\sigma_2 R_{NL} \frac{1+\tan^2\sigma_1}{R_{NL}^2 + Z_1^2 \tan^2\sigma_1} \right) \quad (3)$$

$$\phi = \tan^{-1}\left(\frac{Z_1 \tan\sigma_1}{R_{NL}} \right) \quad (4)$$

The magnitudes and phases of the four voltages at the output of the RF decomposition network, V'_A–V'_D, are plotted as a function of load resistance R_{NL} in Fig. 5. Note that in this plot, $|V_{\text{in}}|$ is held constant. In practice, as will be described below, the value of R_{NL} will vary as a function of $|V_{\text{in}}|$, and the magnitude relationship will therefore be modified from that shown in Fig. 5. Throughout this work we will assume that the PA output amplitudes are equal to each other. The further assumption that they are constant (in the outphasing operating mode) is enforced by both a limiter-based implementation of the nonlinear terminations and the saturating characteristics of the drivers and branch PAs, and will be examined in more detail in the next section.

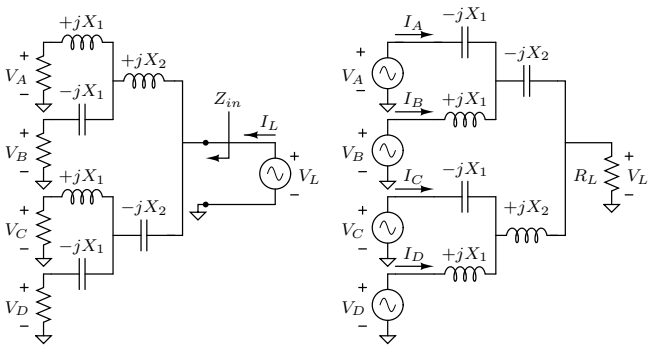

Fig. 4. The dual relationship between RCN and combiner (shown here in lumped-element form) means that wide range output power control of the combiner system is possible through an IRCN control scheme.

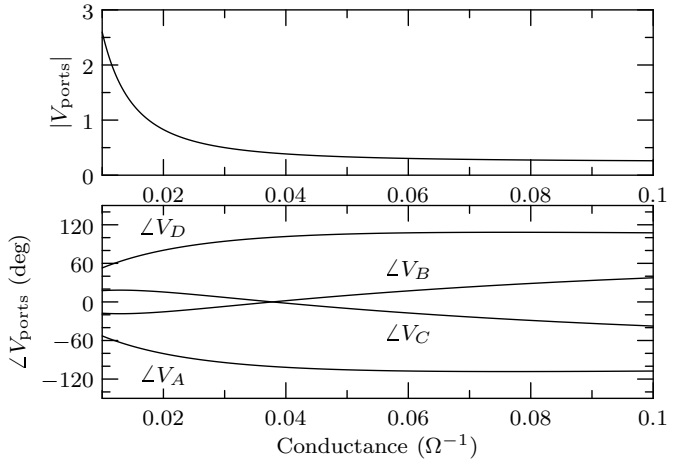

Fig. 5. Plot of the port relationship from (1) when R_{NL} is varied, assuming $|V_{\rm in}|$ is constant, and the decomposition network is designed with parameters $Z_1 = Z_2 = 100\ \Omega$, $\ell_{\rm base} = \lambda/2$, $\Delta_1 = 0.049\lambda$, $\Delta_2 = 0.054\lambda$, and $|V_{\rm in}| = 1$ V. Note that in practice, R_{NL} varies as a function of $|V_{\rm in}|$.

After amplification, the four branch PA outputs (V_A – V_D) (Fig. 3) are assumed to have the same outphasing relationship given by the vector diagram in Fig. 3 and with θ and ϕ from (3)-(4). The magnitudes $|V_A|$ – $|V_D|$ are furthermore assumed to be equal with value V_S. In this case, the output power of the combining system is described by (5) [10].

$$P_{\rm out} = \frac{8R_L V_S^2}{Z_1^2 \sin^2\sigma_1 \cos^2\sigma_2} \sin^2\phi \cos^2\theta \qquad (5)$$

Note that, although the expression for $P_{\rm out}$ is a system property (and therefore unchanged from [10]), the selection of outphasing angles θ and ϕ is different in this work from that of the Optimal Susceptance (OS) control law in [10]. From (5) it can be seen that the output power of the amplifier system can be modulated by controlling either θ and ϕ (through control of R_{NL}), the branch PA drive amplitude $|V_S|$, or a combination of these methods.

The load impedances seen by the four branch PAs is found following the methodology in [10] but with the outphasing angles given by (3)-(4). In this analysis, the magnitudes of the

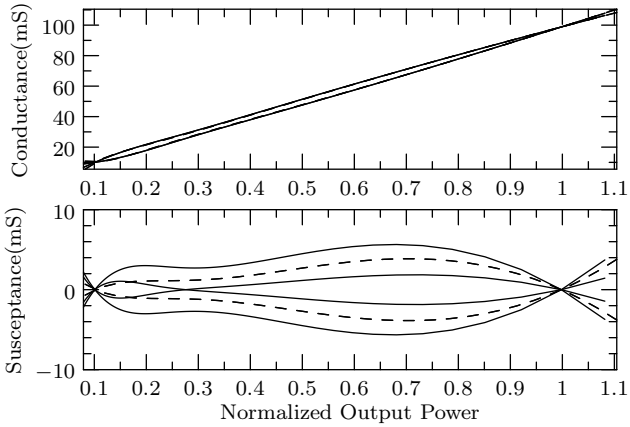

Fig. 6. Plot of the theoretical loading impedances on the ports based on the IRCN (solid) and OS (dashed) control laws for the transmission-line system in this work, assuming a four-way transmission-line power combining as in [10] with values $Z_1 = Z_2 = 100\ \Omega$, $\ell_{\rm base} = \lambda/2$, $\Delta_1 = 0.049\lambda$, $\Delta_2 = 0.054\lambda$, and $R_L = 33\ \Omega$.

four PA outputs V_A–V_D are assumed to be equal and to have a constant value V_S; that is, we ignore any amplitude variation in the PA drive signals due to variation in the amplitudes of V_A'–V_D' (the load impedances seen by the branch PAs do not depend on the value of V_S, only on the relative phases of the four PA outputs). The resulting effective branch PA loading impedances (each including the effect of load modulation from the action of the other PAs) are shown in Fig. 6.

Note that because the RCN and combiner networks are not exact duals, the actual combiner output power does not precisely track the (scaled) input power. However, this and other nonlinearities in the implemented system can be addressed through pre-distortion of the input signal [6], [11], [28].

C. Mixed-Mode Operation

The above system analysis assumes that the branch PAs are operated in saturated or switched mode, with a constant-envelope output voltage and output power control achieved only through modulation of the effective load impedance seen by each PA. In principle, the output power of an outphasing system can be modulated in this way through phase-only control of the multiple signals driving the branch PAs. Practical implementations, however, use both phase and amplitude modulation of the signals driving the branch PAs for two reasons [3], [9]. First, as the system output power is reduced (by increasing the load resistance seen by each branch PA), the input power required to drive each PA into saturation is reduced as well. In this case, drive amplitude modulation can be used to improve efficiency of the overall RF lineup (and power-added efficiency (PAE)) while maintaining outphasing operation [9]. Second, and more importantly for many communications applications, amplitude modulation of the branch PA drive signals can be used to extend the system's output power range to include zero crossings. These two effects are summarized in Fig. 7.

Note that in Fig. 7(a), the individual final stage PAs are operated in compression (and driven into saturation) for most

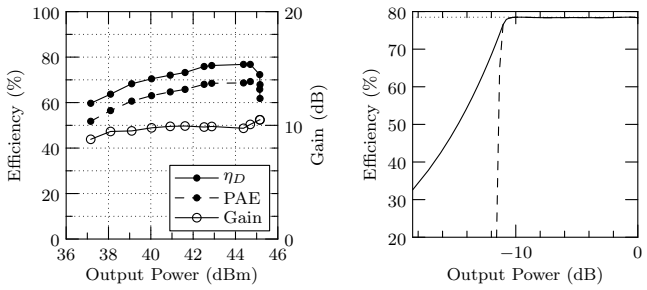

(a) (b)

Fig. 7. Benefits of mixed-mode operation; (a) – measured PAE of the inverse class F PAs used in this work showing PAE over load modulation; PAE is maintained by reducing drive amplitude as the loading impedance increases (reproduced from [9]), (b) – theoretical efficiency of four-way outphasing (assuming branch PAs are implemented in class B) with (solid) and without (dashed) back-off control at low power levels.

of the outphasing range, leading to flat power gain vs. output voltage. However, at the highest output powers / lowest PA loading impedance (owing to load modulation), the drive amplifiers no longer drive the final stage hard enough to saturate it, so the PA comes out of compression and overall power gain increases slightly. Below the shown range, the drive amplitude to the PAs is reduced, and so efficiency is expected to decrease as shown in Fig. 7(b) due to this mixed-mode operation. In the pure outphasing mode (dashed lines in Fig. 7(b)), by contrast, the efficiency drops off in a near-vertical way as a result of operating outside the nominal range of the combiner. The combining network and associated control law is designed for operation over a fixed range (e.g., 10 dB as in Fig. 6), and outside this range the loading impedances of the branch PAs rapidly become highly reactive.

Both Chireix and four-way outphasing systems are designed for a particular dynamic range over which the effective load impedance of the branch PAs is well-controlled, but present highly reactive loads in the limit as the output power goes to zero (resulting in problematic loading conditions for the branch PAs). In practical outphasing systems requiring accurate zero-crossings, therefore, the output power range can be extended by holding the outphasing angles constant at the phases corresponding to the lower extreme of the desired outphasing range, and backing off on the drive amplitudes to operate the branch PAs in a class-B or other non-saturated mode [3], [9]. This approach has the additional advantage that it does not rely on exact cancellation of the outputs of the multiple branch PAs to produce zero output power.

In this work, we realize mixed-mode phase with amplitude modulation through the design of the termination networks at the RCN output ports. In the outphasing mode of operation, the effective loading resistance to the RCN varies over the desired range (i.e., the range of loading impedances that the branch PAs are designed to operate well over). This load resistance variation is a function of input drive amplitude, so that amplitude modulation of the RF input is decomposed into phase modulation for the four branch PA signals. Below the outphasing range, the phases should be held constant at the value corresponding to the low end of the outphasing range, or in other words the effective load resistance seen by the individual PAs becomes fixed. Now amplitude modulation at the input produces amplitude modulation of the branch PA drives. Note that the port impedance derivation in the previous section assumes that the drive amplitudes $|V_A|$–$|V_D|$ are equal, and this operating condition is also maintained in mixed-mode operation.

D. Nonlinear Termination

The amplitude to phase conversion of the decomposition network is produced by realizing its terminations as nonlinear networks whose effective resistance is a function of input power. That is, the variable resistances R_{NL} of Fig. 3 are implemented using nonlinear passive networks having an effective one-port impedance that varies as a function of the applied voltage. At the upper range of input power, the nonlinear loads behave as variable resistors, generating outphasing control angles corresponding to the IRCN control law. Below a threshold level the terminating resistance is fixed and the four signals V_A'-V_D' are amplitude-modulated with the input signal, with the input signal split evenly among the four branches.

The nonlinear load network used in this work is shown in Fig. 8. The implemented impedance variation of the load network is not optimized, but it has the general required characteristics to demonstrate the RF-input outphasing concept, namely that (in the high-power range) the resistance posed by the load network decreases as the power driving it increases. When the applied (sinusoidal) current driving the load network is sufficiently large, the voltage waveform across the load network will be a clipped version of the input current. As the input power is increased, the output voltage will remain at the clipped amplitude, but the fundamental component of the current will increase with input power. As a result, neglecting the effect of R_p and any parasitic resistance, the effective input impedance R_{NL} of this network will be an inverse function of input power. When the parallel resistance R_p is included, then, the input resistance will be limited to a value R_p at low drive (drive levels insufficient to turn on the diodes). The resistor R_p corresponds to an impedance-transformed version of the 50-Ω impedance into the driver amplifiers (Z_δ, Fig. 3).

Fig. 9 shows the simulated amplitude and phase relationships among the four branches when the nonlinear network in Fig. 8 is used to terminate the decomposition network. The mixed-mode outphasing and amplitude control can be clearly seen; below a threshold voltage the outphasing angles are fixed, and the amplitude of the branch voltages is proportional to the input voltage amplitude. Above that threshold, the four voltages V_A'–V_D' follow the IRCN control law. Similarly, the simulated port voltage amplitude (fundamental component only) shows the limiting effects of the diode termination. Note that these voltage signals approach square waves as the drive input level increases, i.e. there is significant additional harmonic content. The driver and RF stage amplifiers also have limiting characteristics, further enforcing constant-envelope behavior at the output of the branch PAs (e.g., the input of the power combining network). The effective load impedances of

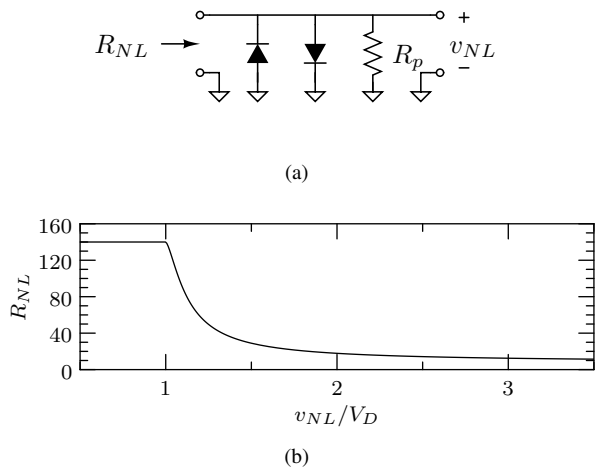

Fig. 8. Nonlinear load element used to terminate the RCN: (a) – equivalent schematic, and (b) – effective input resistance at the fundamental (idealized diode with turn-on voltage V_D and on-resistance $r_d = 8\ \Omega$, $R_p = 140\ \Omega$ assumed).

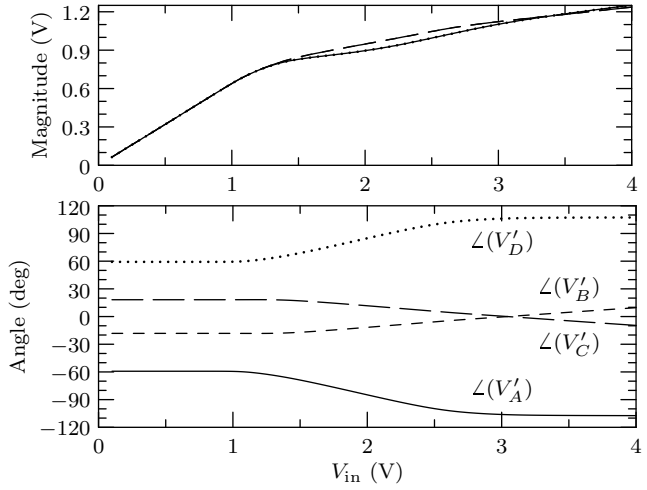

Fig. 9. Simulated amplitude and phase of voltages at the output of the decomposition network, as a function of system input voltage. The mixed-mode outphasing and amplitude control can be seen: between a threshold voltage the outphasing angles are fixed and the amplitude of the branch voltages is proportional to the input voltage. Note that only the fundamental component of the amplitude is shown.

the four branch PAs, shown in Fig. 10, is simulated using the idealized diode-based model.

III. Implementation

This section describes the design and implementation of the RF decomposition network used for experimental validation of the approach, including the implementation of the TLRCN, and the nonlinear loading network. The experimental system is designed to operate at 2.14 GHz.

A. Microstrip TLRCN

The signal decomposition network is implemented as an all-transmission-line RCN [27], although alternative implementa-

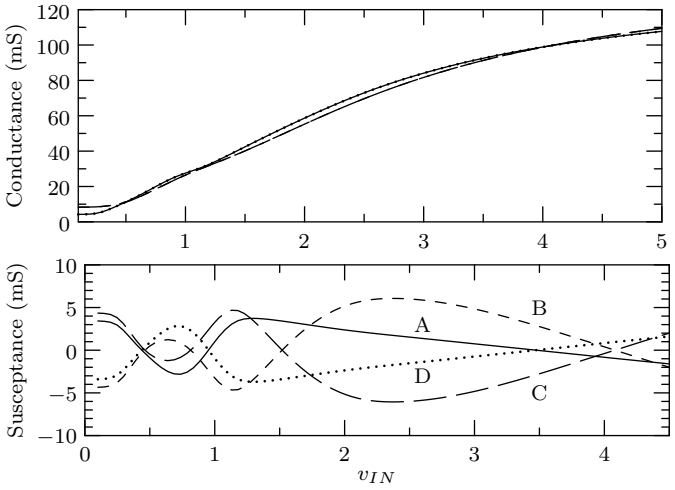

Fig. 10. Effective loading impedances seen by the four branch PAs in the RF-input / RF-output system (Z_ϵ, Figure 3) as a function of system input voltage, when the outphasing angles resulting from the decomposition network are applied to the power combiner (simulated). The diode threshold voltage is simulated as $V_D = 0.2$ V.

tions including could be designed as in the related lumped-element [8] or microstrip [9] power combining networks. The layout (Fig. 11) is made up of curved microstrip segments; right angles and "T" junctions are avoided in order to most closely match the theoretical behavior of the network. The layout of this and other system components are not optimized for size, although more compact versions are possible by using e.g., serpentine layout. This network is implemented on a 1.52-mm thick Rogers RO4350 substrate.

The TLRCN component of the decomposition network is designed assuming that the nonlinear loads vary over an approximately 10–85 Ω range, corresponding to the range that the combining network is designed to present to the branch power amplifiers. The layout therefore uses the same parameters as the power combining network [10], with characteristic impedances $Z_1 = Z_2 = 100\ \Omega$, and delta-electrical lengths $\Delta_1 = 0.049\lambda$ and $\Delta_2 = 0.054\lambda$. (The original paper describing the transmission-line combiner [10] indicated values $\Delta_1 = 0.201\lambda$ and $\Delta_2 = 0.196\lambda$ in error; the lengths $\Delta_1 = 0.049\lambda$ and $\Delta_2 = 0.054\lambda$ were used in both the transmission-line combiner and TLRCN.)

A secondary benefit of the TLRCN structure is that it provides a narrow-range resistive input impedance even when its load impedances (Z_2, Fig. 3) vary. As in the corresponding combiner design, an impedance-transforming quarter-wave transmission line is included at the input port, with $Z_T = 40.8\ \Omega$. Combined with the resistance compression behavior of the TLRCN, this impedance transformation establishes a nominally 50-Ω input impedance to the power amplifier system. The simulated reflection coefficient at the input port has $|S_{11}| < -30$ dB over the entire range of operation.

B. Nonlinear Load Element

The anti-parallel diode pair is implemented using Avago HSMS-286C detector diodes, which are available as a single

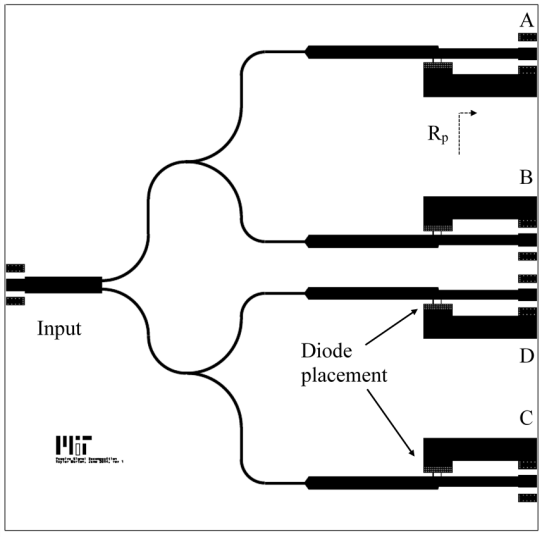

Fig. 11. Layout of RF signal decomposition board implemented on a 1.52-mm-thick Rogers RO4350 substrate. The board dimensions are 14.5 cm x 14.2 cm. As indicated, the parallel resistance R_p is synthesized from the (50-Ω) impedance into the driver stage using a quarter-wavelength impedance transformation.

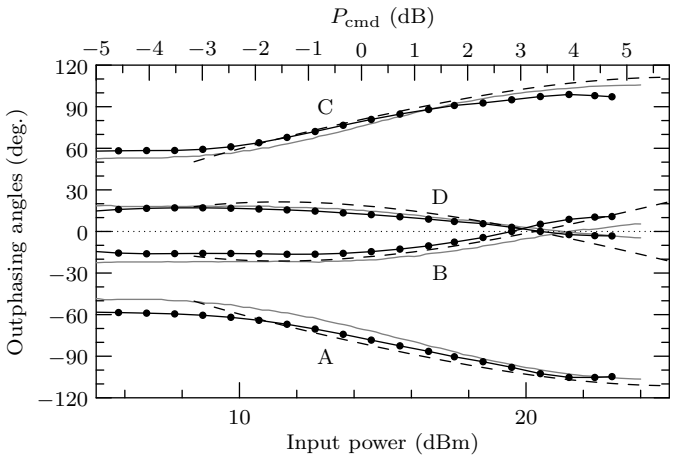

Fig. 12. Comparison of measured relative phases at the outputs of the decomposition network (grey), the full PA paths (black; branch PAs 50-Ω terminated), and the ideal phase relationship calculated based on commanded power using the optimal susceptance control law [10] (dashed, top axis). Net phase shift has been removed from the plot for clarity. The mixed-mode behavior can be seen below around 7 dB input commanded power, below which the measured outphasing angles are held constant.

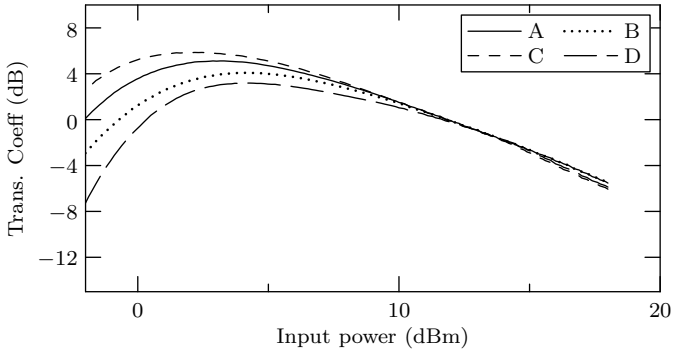

Fig. 13. Measured transmission coefficient (normalized) of each PA path (terminated by 50 Ω) as a function of system input power. The variation in AM/AM performance between the four paths was not corrected for in the system characterization.

packaged pair. Matching to reduce the effects of parasitic reactance is incorporated into the quarter-wavelength transmission line before the diode. For other choices of diodes or frequency, a more complicated impedance match may be necessary. The shunt resistance R_p is designed to be 85 Ω, and is generated by transforming the 50 Ω input impedance of the following (driver) stage with a quarter-wavelength impedance transformer.

IV. Experimental System

A. Decomposition Network

The decomposition network is characterized by measuring the phase relationship at its four output ports (ports A, B, C, D in Fig. 11) when the input power is varied. For this experiment, the decomposition network is first terminated (at reference plane D, Fig. 3) with 50-Ω loads representing the input impedances to the PA drivers. The relative phases at the four output ports of the decomposition network (V'_A–V'_D) are shown in Fig. 12 (grey curves). This figure shows the relative phases among the four branches only; net phase shift has been removed from the plot for clarity. Next, the full RF paths are characterized up to reference plane E; for this measurement, the branch PAs are terminated in 50 Ω and the relative phase of signals V_A–V_D at their outputs is characterized with system input power (Fig. 12, black curves). Note that the actual phase relationship into the combiner may vary if the PAs have load-modulation to phase-modulation nonlinearity. Static phase offsets are trimmed out using phase shift tuners (Aeroflex Weinchsel 980-4) in the four paths. The transition between outphasing control and drive modulation can also be seen near 7 dB normalized input power.

The measured phase characteristics are compared to those calculated from the OS control law (which in principle yields more optimal performance than the IRCN control law), shown in Fig. 12 as dashed curves (and referring to the top axis). A close match can be observed between the phase relationships among the measured and theoretical control angles. At the same time, it can be seen by comparing the top and bottom axes that there is not a one-to-one correlation between the two scales, and that the input power range of the experimental system is approximately twice (in dB) that of the calculated power command range. This means that the output power is not a linear function of linear power (as will be shown in the system measurements below); this nonlinearity is related to the implementation of the nonlinear load network used in this work.

The amplitude characteristics of all four ports are likewise measured over swept input power. This measurement, made into 50 Ω loads only, reveals amplitude mismatch among the four branches, particularly at low drive levels (see Fig. 13). This imbalance was not corrected for in the system characterization.

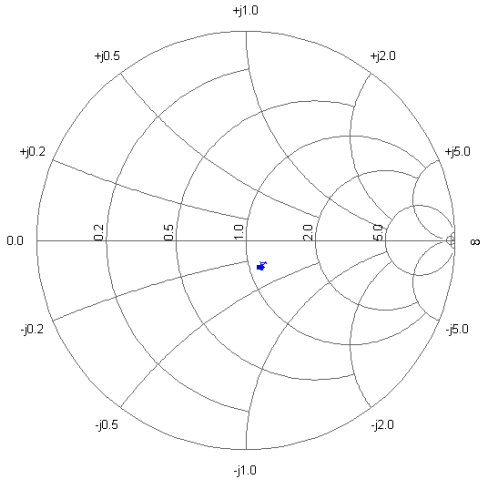

Fig. 14. Input reflection coefficient for the signal decomposition network as the input power is swept over the 20-dB range as in Fig. 12. This measurement corresponds to the reference plane indicated by Z_α in Fig. 3. The nearly constant input impedance (showing $|\Gamma| < 0.17$) is a result of the resistance compression network used as the basis for the signal decomposition network.

The resistance compression property of the decomposition network can be seen in Fig. 14, which shows the measured input impedance to the RF decomposition network (Z_α in Fig. 3) over the swept power characterization of Fig. 12. The input reflection coefficient remains better than $|\Gamma| < 0.17$ over the entire range of applied power. Furthermore, the impedance is nearly constant, with an improved 50-ohm match clearly possible if desired.

B. RF-input / RF-output Outphasing System

1) Overview: A photograph of the complete system including (left to right) the decomposition network, phase shift tuners, two predriver stages, the inverse class F branch PAs, and the power combining network [10], is shown in Fig. 15. The input CW or W-CDMA signal is generated using a Rohde & Schwarz SMJ100A vector signal generator, and is amplified by a pre-amplifier to reach the required input level before the signal decomposition network. The nature of the nonlinear loads in the decomposition network constrains the possible range of input powers to the system for a given design. Here, the decomposition network is designed for input powers up to 23 dBm, while a 50 dBm system output power is desired. After the RF-domain decomposition, phase-shift tuners are employed to trim out static phase offsets (these are largely due to mismatched delays in the driver amplifiers). The two driver amplifiers, based on demonstration boards for the Hittite HMC455 and Freescale MW7IC2020N parts respectively, have not been optimized for the system, and so are excluded from the efficiency characterization. In fact, as can be seen in the photograph, excess gain in the driver chain is adjusted for using fixed attenuators. This arrangement is due to the available driver stages and is clearly undesirable for a practical system. Note that the driver PAs have been replaced compared to the related work in [26], although efficiency performance is similar. The branch PAs are based on the CGH40025 device

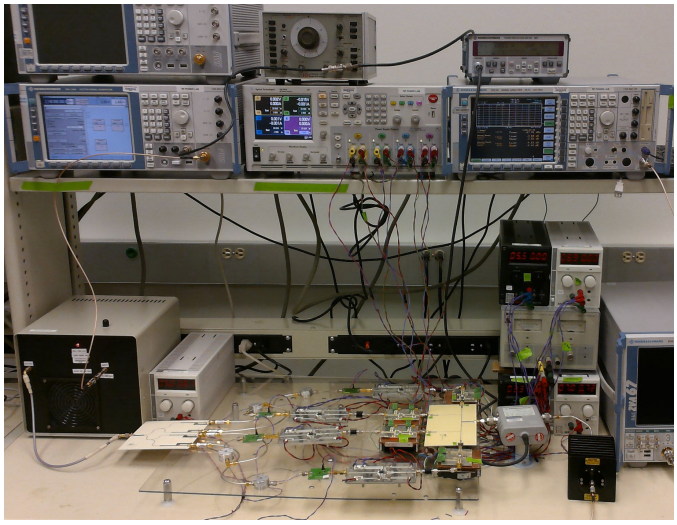

(a)

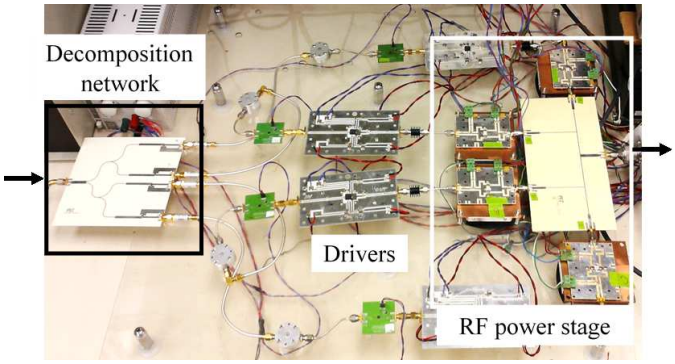

(b)

Fig. 15. System photograph showing: (a) – the testbench including instrumentation; (b) – details of the RF decomposition network, drivers, and RF power stage.

from CREE and the design in [14], and are the same PAs as used in the baseband-input work demonstrating the all-transmission-line multi-way outphasing power combiner [10]. The power combining network is likewise the same as used in [10], so that the performence of that baseband-input system can be directly compared to this work. Drain efficiency of the final-stage power amplifiers (which have approximately 10 dB gain [9]) is measured using an Agilent N6705A power supply and Rohde & Schwarz NRT power meter. A block diagram of the measurement setup is shown in Fig. 16.

2) CW Measurements: A CW measurement of drain efficiency of the final RF power stage vs. output power is shown in Fig. 17 (black curve). The power amplifier has a peak output power of 49.7 dBm and peak drain efficiency of 70%. Also shown (grey curve) is a system characterization in which the branch PA drive signals (corresponding to reference plane E in Fig. 3) are generated using four separate *IQ* modulators with the Optimal Susceptance control law that selects outphasing angles such that the reactive component of the branch PA load impedance is minimized (reproduced from [10]). The same combiner and RF power stage are used for both measurements. Note that the inclusion of phase shift tuners compared to the

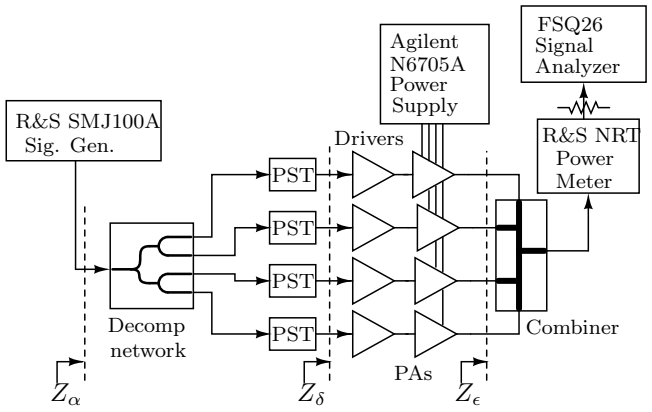

Fig. 16. Block diagram of the measurement setup, with reference planes indicated based on the definitions in Fig. 3.

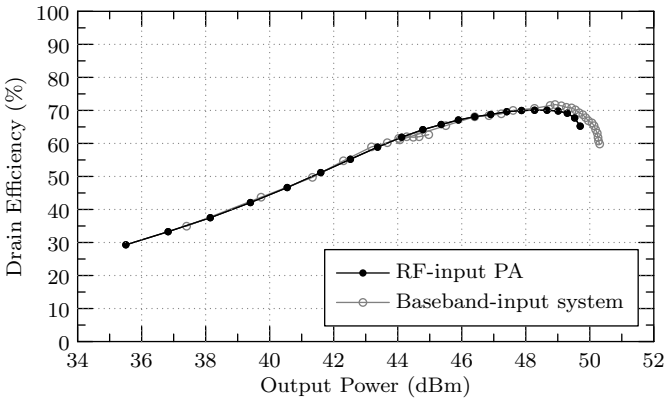

Fig. 17. Measured outphasing power amplifier performance (black), and measured performance of a baseband-input system comprising the same branch PAs and power combining network [10]. The new RF-input PA has nearly identical performance but operates directly on a modulated RF signal with a simple passive network replacing the complex baseband signal processing setup of [10]. This variation occurs due to differences in the active devices, passive devices, interconnects and pcb manufacturing among the PA and driver chains of the four paths.

initial prototype in [26] allows for static phase adjustment of the four paths and a slightly improved efficiency characteristic.

The excellent match in the efficiency performance of these systems demonstrates the effectiveness of the RF signal decomposition network. The reduced peak power of the new system is likely due to a combination of the higher load susceptance associated with the IRCN law and the phase mismatch observed in Fig. 12. Compared to the system using four *IQ* modulators, this proof-of-concept RF-input / RF-output implementation has significant advantages in system complexity without degradation in peak efficiency.

The RF-input / RF-output outphasing amplifier is also characterized in terms of CW input/output characteristics as shown in Fig. 18. The two regions of output power control, amplitude modulation and outphasing control, are apparent from this measurement. The clear "knee" between the two regimes, and the compressive behavior in the outphasing control region, indicate that the nonlinear termination R_{NL} for this design is not optimal. This and other nonlinearities can be addressed

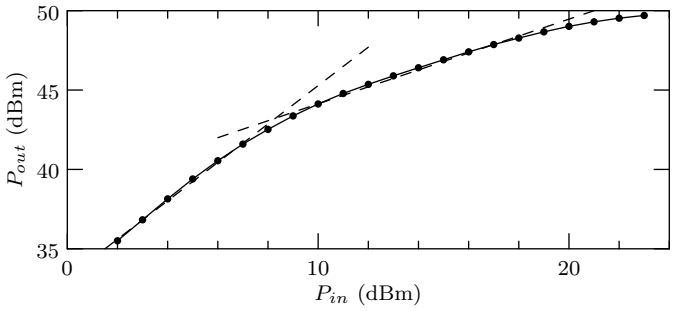

Fig. 18. CW characterization of the power amplifier. The inflection point at the transition between outphasing and amplitude modulation for output power control can be seen around an output power of approximately 44 dBm.

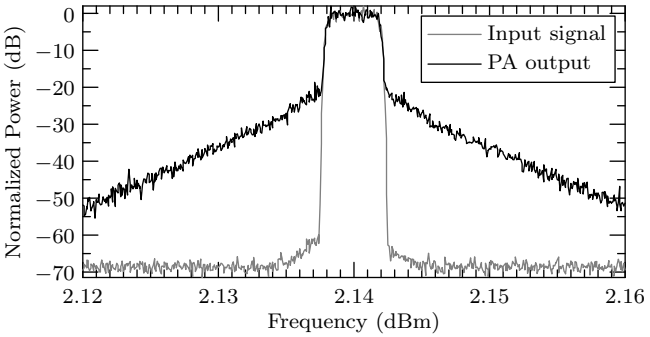

Fig. 19. Output spectrum of the RF-input outphasing PA when no linearization is applied, measured over a 40 MHz span for a 3.84 MHz W-CDMA signal.

TABLE I
COMPARISON TO OTHER WORKS: W-CDMA PERFORMANCE

Ref.	Arch.	RF in	Carrier (MHz)	P_{max} (W)	PAPR (dB)	$ACLR_1$ (dBc)	Drain Eff.
[29]	Chireix	No	2300	70	9.6	-49	53.5%
[3]	Chireix	No	2140	90	9.6	-47	50.5%
[4]	Chireix	No	1950	19	9.6	-47	54.5%
[14]	4-way Doherty	Yes	2140	100	6.5	-31*	61%
[30]	Saturated Doherty	Yes	2140	10	7.4	-28.3*	52.4%
[9]	4-way Radial	No	2140	110	9.15	-33.0	55.6%
[10]	4-way TL	No	2140	105	9.	-34.2	54.5%
This Work	RF-in 4-way	Yes	2140	93	6.18	-24*	65%

* no predistortion

through pre-distortion of the input signal or further refinement of the nonlinear load characteristic used in the decomposition network.

3) Modulated Measurements: A preliminary characterization of the outphasing PA was performed using a W-CDMA input signal. The measured output spectrum, with no linearization applied, is shown in Fig. 19. For this measurement, the average output power was 24 W, and average drain efficiency of the final PA stage was $\eta_{D,\text{avg}} = 65\%$. The measured output PAPR was 6.18 dB. A comparison to other works of related technology and power level is given in Table I.

The evident nonlinearity of the RF-input outphasing PA may be attributed to several factors including the nonlinear overall

AM-AM characteristic shown in Fig. 18, which is most likely caused by the non-ideal nonlinear termination element R_{NL} used in the implemented system. Improvements in this nonlinear characteristic, along with a complete characterization of the load-modulation-to-amplitude-modulation characteristics of the branch PAs, could improve the observed "knee" characteristic in Fig. 18. The linearity of outphasing systems has additionally been shown to be sensitive to amplitude, phase, and delay mismatch among the branches, and limited bandwidth of the combining network [31]–[33]. We note that a common linearization approach for outphasing systems (e.g., [32], [33]) treats the signal component separator, branch PAs, and power combining network as a "black box" model, and applies digital predistortion (DPD) based on the overall input-output characteristic of the system. Although linearization is outside the scope of this work, which focuses on the initial proof-of-concept demonstration of RF-input outphasing, we therefore expect that this architecture is compatible with conventional linearization techniques.

V. Conclusion

The RF signal decomposition network presented in this work exploits the relationship between resistance compression networks and lossless outphasing power combiners in order to create an RF-input / RF-output outphasing power amplifier. This approach eliminates the digital signal component separator and multiple *IQ* modulators required for prior outphasing system implementations. Advantages of the approach include reduced system cost and baseband signal processing complexity, and the ability to work with many existing calibration and digital pre-distortion schemes.

The proof-of-concept prototype in this work is implemented using transmission-line techniques, and demonstrates the feasibility of this approach through CW measurements at 2.14 GHz. The system achieves a peak output power of 93 W and a peak drain efficiency of 70%, performance that is on par with the previously-demonstrated outphasing system [10] requiring four *IQ* modulators. The excellent match between these two systems demonstrates the effectiveness of the RF signal decomposition approach. This approach can be extended to a range of frequencies and implementation types including lumped element implementations as in [8], or microstrip versions [9]. Future development of this technique will focus on design of the nonlinear termination in the signal decomposition network to generate a more overall-linear characteristic.

Appendix

This appendix gives the derivation of (1)–(4) relating the port voltages of the decomposition network when the terminating impedance R_{NL} varies.

The three-port network shown in Fig. 20 can be thought of as the fundamental building block of both the transmission-line-based power combining network and the TLRCN. The port relationship of this network can be shown through transmission-line analysis to be:

$$\begin{bmatrix} I_1 \\ I_2 \\ I_3 \end{bmatrix} = \frac{j}{Z_0 \sin\sigma} \begin{bmatrix} -\cos\sigma & 0 & -1 \\ 0 & \cos\sigma & 1 \\ -1 & 1 & 0 \end{bmatrix} \begin{bmatrix} V_1 \\ V_2 \\ V_3 \end{bmatrix} \tag{6}$$

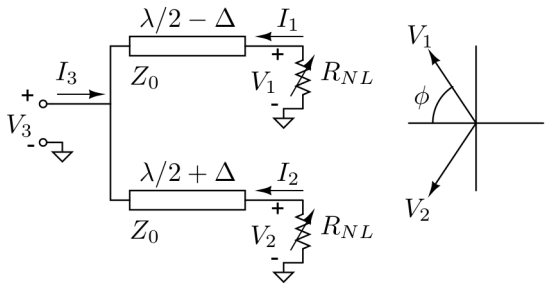

Fig. 20. Three-port network forming the building blocks of both the transmission-line combining network and the TLRCN-based decomposition network.

where $\sigma = 2\pi\Delta/\lambda$.

When ports 1 and 2 are terminated resistively, $V_{1,2}/I_{1,2} = -R_{NL}$, the port voltages can be written as:

$$V_1 = V_3 \frac{jR_{NL}}{Z_0 \sin\sigma - jR_{NL}\cos\sigma} \tag{7}$$

$$V_2 = V_3 \frac{-jR_{NL}}{Z_0 \sin\sigma + jR_{NL}\cos\sigma} \tag{8}$$

In this application, the parameters of interest are the magnitude of port voltages V_1 and V_2, and the relative phase between the ports. The voltage magnitudes are equal and given by (9), while the two port phases are given by (10)–(11).

$$|V_{1,2}| = |V_3| \frac{R_{NL}}{\sqrt{Z_0^2 \sin^2\sigma + R_{NL}^2 \cos^2\sigma}} \tag{9}$$

$$\angle V_1 = \frac{\pi}{2} + \tan^{-1}\left(\frac{R_{NL}}{Z_0 \tan\sigma}\right) \tag{10}$$

$$\angle V_2 = -\frac{\pi}{2} - \tan^{-1}\left(\frac{R_{NL}}{Z_0 \tan\sigma}\right) \tag{11}$$

When ϕ is as defined graphically in Fig. 20, then, this outphasing angle can be written as:

$$\phi = \tan^{-1}\left(\frac{Z_0 \tan\sigma}{R_{NL}}\right) \tag{12}$$

To form the four-way decomposition network, the stage in Fig. 20 is "stacked" in a coporate combining structure. The behavior of the second stage is identical to the first, and it is loaded with a variable resistance (Z_β in Fig. 3) that is a function of R_{NL}. This impedance Z_β is the input impedance to the first stage (Z_3 in Fig. 20) and can be calculated following the analysis in [27] to be:

$$Z_3 = Z_\beta = \frac{1}{2R_{NL}} \frac{R_{NL}^2 + Z_0 \tan^2\sigma}{1 + \tan^2\sigma} \tag{13}$$

The relative angle θ resulting at the plane indicated by Z_β in Fig. 3 is obtained by substituting the expression for Z_3 into (12), producing equation (3)):

$$\theta = \tan^{-1}\left(Z_0 \tan\sigma_2 \cdot 2R_{NL} \frac{1 + \tan^2\sigma_1}{R_{NL}^2 + Z_0 \tan^2\sigma_1}\right) \tag{14}$$

As shown in Fig. 3, we denote the segments closer to R_{NL} as having differential electrical length Δ_1, and the segment closer to the input as having differential electrical length Δ_2.

The port voltage magnitudes after the second stage (i.e., at the reference plane indicated by Z_β in Fig. 3) can be found by substituting the expression for Z_3 into (9):

$$|V_3| = |V_{\text{in}}| \frac{Z_3}{\sqrt{Z_0^2 \sin^2 \sigma_2 + Z_3^2 \cos^2 \sigma_2}} \tag{15}$$

Substituting (15) into (9) yields the port voltage amplitude given in (1).

REFERENCES

[1] H. Chireix, "High power outphasing modulation," *Proceedings of the IRE*, vol. 23, no. 11, pp. 1370–1392, Nov. 1935.

[2] D. Calvillo-Cortes, M. van der Heijden, M. Acar, M. de Langen, R. Wesson, F. van Rijs, and L. de Vreede, "A package-integrated Chireix outphasing RF switch-mode high-power amplifier," *IEEE Trans. Microw. Theory Techn.*, vol. 61, no. 10, pp. 3721–3732, Oct 2013.

[3] J. Qureshi, M. Pelk, M. Marchetti, W. Neo, J. Gajadharsing, M. van der Heijden, and L. de Vreede, "A 90-W peak power GaN outphasing amplifier with optimum input signal conditioning," *IEEE Trans. Microw. Theory Techn.*, vol. 57, no. 8, pp. 1925–1935, Aug. 2009.

[4] M. van der Heijden, M. Acar, J. Vromans, and D. Calvillo-Cortes, "A 19W high-efficiency wide-band CMOS-GaN class-E Chireix RF outphasing power amplifier," in *IEEE MTT-S Int. Microw. Symp. (IMS)*, June 2011, pp. 1–4.

[5] M. Pampin-Gonzalez, M. Ozen, C. Sanchez-Perez, J. Chani-Cahuana, and C. Fager, "Outphasing combiner synthesis from transistor load pull data," in *IEEE MTT-S Int. Microw. Symp. (IMS)*, May 2015, pp. 1–4.

[6] D. Perreault, "A new power combining and outphasing modulation system for high-efficiency power amplification," *IEEE Trans. Circuits Syst. I: Reg. Papers*, vol. 58, no. 8, pp. 1713–1726, Feb. 2011.

[7] A. Jurkov, L. Roslaniec, and D. Perreault, "Lossless multi-way power combining and outphasing for high-frequency resonant inverters," in *2012 Int. Power Electron. Motion Control Conf.*, vol. 2, June 2012, pp. 910–917.

[8] T. Barton, J. Dawson, and D. Perreault, "Experimental validation of a four-way outphasing combiner for microwave power amplification," *IEEE Microw. Wireless Compon. Lett.*, vol. 23, no. 1, pp. 28–30, Jan. 2013.

[9] T. Barton and D. Perreault, "Four-way microstrip-based power combining for microwave outphasing power amplifiers," *IEEE Trans. Circuits Syst. I: Reg. Papers*, vol. 61, no. 10, pp. 2987–2998, Oct 2014.

[10] T. W. Barton, A. S. Jurkov, and D. J. Perreault, "Transmission-line-based multi-way lossless power combining and outphasing system," in *IEEE MTT-S Int. Microw. Symp. (IMS)*, June 2014, pp. 1–4.

[11] A. Jurkov, L. Roslaniec, and D. Perreault, "Lossless multi-way power combining and outphasing for high-frequency resonant inverters," *IEEE Trans. Power Electron.*, vol. 29, no. 4, pp. 1894–1908, April 2014.

[12] A. Miller and J. Novik, "Principles of operation of the Ampliphase transmitter," *Broadcast News*, no. 104, June 1959.

[13] W. Doherty, "A new high efficiency power amplifier for modulated waves," *Proceedings of the Institute of Radio Engineers*, vol. 24, no. 9, pp. 1163 – 1182, sept. 1936.

[14] A. Grebennikov, "A high-efficiency 100-W four-stage Doherty GaN HEMT power amplifier module for WCDMA systems," in *IEEE MTT-S Int. Microw. Symp. (IMS)*, June 2011, pp. 1–4.

[15] L. Panseri, L. Romano, S. Levantino, C. Samori, and A. Lacaita, "Low-power signal component separator for a 64-QAM 802.11 LINC transmitter," *IEEE Journal Solid-State Circuits*, vol. 43, no. 5, pp. 1274–1286, May 2008.

[16] A. Rustako and Y. Yeh, "A wide-band phase-feedback inverse-sine phase modulator with application toward a LINC amplifier," *IEEE Trans. Communications*, vol. 24, no. 10, pp. 1139–1143, Oct 1976.

[17] D. Cox and R. Leck, "Component signal separation and recombination for linear amplification with nonlinear components," *IEEE Trans. Communications*, vol. 23, no. 11, pp. 1281–1287, Nov 1975.

[18] B. Shi and L. Sundstrom, "A 200-MHz IF BiCMOS signal component separator for linear LINC transmitters," *IEEE Journal Solid-State Circuits*, vol. 35, no. 7, pp. 987–993, July 2000.

[19] ——, "A translinear-based chip for linear LINC transmitters," in *Symp. on VLSI Circuits*, June 2000, pp. 58–61.

[20] L. Sundstrom, "The effect of quantization in a digital signal component separator for LINC transmitters," *IEEE Trans. Vehicular Tech.*, vol. 45, no. 2, pp. 346–352, May 1996.

[21] S. Hetzel, A. Bateman, and J. McGeehan, "A LINC transmitter," in *IEEE Vehicular Tech. Conf.*, May 1991, pp. 133–137.

[22] W. Gerhard and R. Knoechel, "LINC digital component separator for single and multicarrier W-CDMA signals," *IEEE Trans. Microw. Theory Techn.*, vol. 53, no. 1, pp. 274–282, Jan 2005.

[23] Y. Li, Z. Li, O. Uyar, Y. Avniel, A. Megretski, and V. Stojanovic, "High-throughput signal component separator for asymmetric multi-level outphasing power amplifiers," *IEEE Journal of Solid-State Circuits*, vol. 48, no. 2, pp. 369–380, Feb 2013.

[24] T.-W. Chen, P.-Y. Tsai, D. De Moitie, J.-Y. Yu, and C.-Y. Lee, "A low power all-digital signal component separator for uneven multi-level LINC systems," in *Proc. European Solid-State Circuits Conference*, Sept 2011, pp. 403–406.

[25] M. Heidari, M. Lee, and A. Abidi, "All-digital outphasing modulator for a software-defined transmitter," *IEEE Journal of Solid-State Circuits*, vol. 44, no. 4, pp. 1260–1271, April 2009.

[26] T. Barton and D. Perreault, "An RF-input outphasing power amplifier with RF signal decomposition network," in *IEEE MTT-S Int. Microw. Symp. (IMS)*, May 2015, pp. 1–4.

[27] T. Barton, J. Gordonson, and D. Perreault, "Transmission line resistance compression networks and applications to wireless power transfer," *IEEE Journal of Emerging and Selected Topics in Power Electronics*, vol. 3, no. 1, pp. 252–260, March 2015.

[28] A. Jurkov and D. Perreault, "Design and control of lossless multi-way power combining and outphasing systems," in *Midwest Symp. Circuits Syst.*, Aug. 2011, pp. 1–4.

[29] D. Calvillo-Cortes, M. van der Heijden, and L. de Vreede, "A 70W package-integrated class-E Chireix outphasing RF power amplifier," in *IEEE MTT-S Int. Microw. Symp. (IMS)*, June 2013, pp. 1–3.

[30] J. Kim, J. Moon, Y. Y. Woo, S. Hong, I. Kim, J. Kim, and B. Kim, "Analysis of a fully matched saturated Doherty amplifier with excellent efficiency," *IEEE Trans. Microw. Theory Techn.*, vol. 56, no. 2, pp. 328–338, 2008.

[31] T. Hwang, K. Azadet, R. Wilson, and J. Lin, "Linearization and imbalance correction techniques for broadband outphasing power amplifiers," *IEEE Trans. Microw. Theory Techn.*, vol. 63, no. 7, pp. 2185–2198, July 2015.

[32] P. Landin, J. Fritzin, W. Van Moer, M. Isaksson, and A. Alvandpour, "Modeling and digital predistortion of class-d outphasing rf power amplifiers," *IEEE Trans. Microw. Theory Techn.*, vol. 60, no. 6, pp. 1907–1915, June 2012.

[33] A. Aref, T. Hone, and R. Negra, "A study of the impact of delay mismatch on linearity of outphasing transmitters," *IEEE Trans. Circuits Syst. I: Reg. Papers*, vol. 62, no. 1, pp. 254–262, Jan 2015.

Taylor W. Barton (S'07, M'12) received the Sc. B., M.Eng., E.E., and Sc.D degrees from the Massachusetts Institute of Technology, Cambridge, MA in 2012. In 2014 she joined The University of Texas at Dallas, where she is currently an Assistant Professor. Prior to joining joining UT Dallas, she was a Postdoctoral Associate in the MIT Microsystems Technology Laboratories. Her research interests include high-efficiency RF, power, and analog circuit design, and classical control theory.

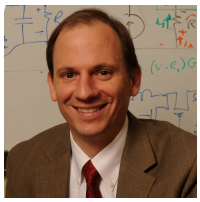

David J. Perreault (S'91, M'97, SM'06, F'13) received the B.S. degree from Boston University, Boston, MA, and the S.M. and Ph.D. degrees from the Massachusetts Institute of Technology, Cambridge, MA. In 1997 he joined the MIT Laboratory for Electromagnetic and Electronic Systems as a Postdoctoral Associate, and became a Research Scientist in the laboratory in 1999. In 2001, he joined the MIT Department of Electrical Engineering and Computer Science, where he is presently Professor and Associate Department Head. His research interests include design, manufacturing, and control techniques for power electronic systems and components, and in their use in a wide range of applications. He also consults in industry, and is co-founder of Eta Devices, a startup company focusing on high-efficiency RF power amplifiers. Dr. Perreault received the Richard M. Bass Outstanding Young Power Electronics Engineer Award, the R. David Middlebrook Achievement Award, the ONR Young Investigator Award, and the SAE Ralph R. Teetor Educational Award, and is co-author of seven IEEE prize papers.